ASME Journal of Biomechanical Engineering
Online journal at:
https://asmedigitalcollection.asme.org/biomechanical

Huizhou Yang[1]
Center for Orthopaedic Biomechanics,
University of Denver,
Room 434, 2155 E. Wesley Avenue,
Denver, CO 80208
e-mail: Huizhou.yang@du.edu

Daniele Marras
Center for Orthopaedic Biomechanics,
University of Denver,
Denver, CO 80208

Chadd W. Clary
Center for Orthopaedic Biomechanics,
University of Denver,
Denver, CO 80208

Thomas Zumbrunn
Institute for Biomechanics,
ETH Zurich,
Hönggerbergring 64, HPP O14,
Zurich 8093, Switzerland

Renate List
Institute for Biomechanics,
ETH Zurich,
Hönggerbergring 64, HPP O14,
Zurich 8093, Switzerland;
Human Performance Lab,
Schulthess Clinic,
Zurich 8008, Switzerland

Stephen J. Ferguson
Institute for Biomechanics,
ETH Zurich,
Hönggerbergring 64, HPP O14,
Zurich 8093, Switzerland

Paul J. Rullkoetter[1]
Center for Orthopaedic Biomechanics,
University of Denver,
Room 427, 2155 E. Wesley Avenue,
Denver, CO 80208
e-mail: paul.rullkoetter@du.edu

Impact of Surgical Alignment, Bone Properties, Anterior–Posterior Translation, and Implant Design Factors on Fixation in Cementless Unicompartmental Knee Arthroplasty

Micromotion exceeding 150 μm at the implant–bone interface may prevent bone formation and limit fixation after cementless knee arthroplasty. Understanding the critical parameters impacting micromotion is required for optimal implant design and clinical performance. However, few studies have focused on unicompartmental knee arthroplasty (UKA). This study assessed the impacts of alignment, surgical, and design factors on implant–bone micromotions for a novel cementless UKA design during a series of simulated daily activities. Three finite element models that were validated for predicting micromotion of cementless total knee arthroplasty (TKA) were loaded with design-specific kinematics/loading to simulate gait (GT), deep knee bending (DKB), and stair descent (SD). The implant–bone micromotion and the porous surface area ideal for bone ingrowth were estimated and compared to quantify the impact of each factor. Overall, the peak tray–bone micromotions were consistently found at the lateral aspect of the tibial baseplate and were consistently higher than the femoral micromotions. The femoral micromotion was insensitive to almost all the factors studied, and the porous area favorable for bone ingrowth was no less than 93%. For a medial uni, implanting the tray 1 mm medially or the femoral component 1 mm laterally reduced the tibial micromotion by 19.3% and 26.3%, respectively. Differences in tray–bone micromotion due to bone moduli were up to 59.8%. A 5 mm more posterior femoral translation increased the tray–bone micromotion by 35.8%. The presence of the tray keel prevented the spread of the micromotion and increased the overall porous surface area, but also increased peak micromotion. The tray peg and the femoral anterior peg had little impact on the micromotion of their respective implants. In conclusion, centralizing the load transfer to minimize tibial tray applied moment and optimizing the fixation features to minimize micromotion are consistent themes for improving cementless fixation in UKA. Perturbation of femoral–bone alignment may be preferred as it would not create under/overhang on the tibia. [DOI: 10.1115/1.4066969]

Keywords: unicompartmental knee arthroplasty, cementless, micromotion, fixation, finite element analysis

1 Introduction

Unicompartmental knee arthroplasty (UKA) is a minimally invasive alternative to total knee arthroplasty (TKA) that only replaces the diseased compartment (most commonly in the medial) and preserves the remaining native knee joint [1,2]. UKA has shown shorter operative times, faster rehabilitation, additional preserved bone stock for revision, and similar kinematics to native knees compared with TKA [3–5]. However, due to the higher revision rate [6,7], UKA use remains less than 10% of TKA, although 47% of patients are eligible [8]. One of the most common reasons for UKA failure and the conversion to a TKA is aseptic loosening [9–12]. Cementless UKA was introduced to reduce the rates of aseptic tibial loosening and improve long term fixation [9]. Although there is

[1]Corresponding authors.

Manuscript received June 12, 2024; final manuscript received October 14, 2024; published online November 20, 2024. Assoc. Editor: Hannah Dailey.

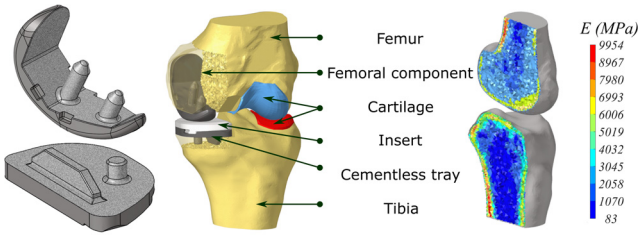

Fig. 1 (*a*) The fixed-bearing cementless designs and (*b*) computational model setup (left knee sample)

historically no significant difference in the outcomes between cemented and cementless UKA [13,14], recent innovations in cementless components could offer a more long-lasting biological fixation [15,16]. The primary fixation strength in cementless prostheses depends upon bony ingrowth onto the porous surface of the implant [17], as micromotion exceeding 150 μm may inhibit bone formation and lead to implant loosening [18,19]. Therefore, understanding the critical parameters impacting micromotion in cementless UKA is critical for optimal design, patient selection, and clinical performance.

Many in vitro experiments have been performed to investigate the impact of various factors on implant–bone micromotion in TKA [20–22]. However, only a limited number of studies have focused on UKA [23,24]. Reiner et al. (2014) compared the micromotion of the femoral component between single-peg and twin-peg designs and reported equivalent fixation stability for the two groups [23]. Yildirim et al. (2016) investigated the impact of fixation features on tibial micromotions using synthetic bones and found the L-shaped keel design best resisted micromotion [24]. These studies measured and compared the relative displacements between markers placed on the exposed surfaces of the implant and bone. However, these measurements are limited to a few distinct points, which may not correspond to the actual peak interface micromotions. Also, the boundary conditions used in these studies were simple compressive loads applied at certain knee flexion angles, which do not account for the complex physiological loading at the knee joint during daily activities.

Finite element models have been commonly used to estimate interface micromotion that cannot be measured experimentally. Once validated, they can be used to further investigate factors or compare different designs. Our prior experimental–computational studies have presented validation of predicted implant–bone micromotions in cementless TKA and investigated the influence of TKA factors on micromotion [25–27]. Previous studies have reported that implant alignments, bone properties, and fixation features could have a significant impact on micromotion in cementless TKA [20–22,26,27]. To our knowledge, no previous studies have systematically studied the sensitivity of the implant–bone micromotion to these factors in UKA under physiological conditions.

Hence, this study aimed to investigate the impact of implant alignment, bone material properties, tibiofemoral anterior–posterior (AP) translations, and implant design factors on femoral–bone and tray–bone interface micromotions in cementless UKA during a series of daily activities. Factors were studied using three knee models (tibia models previously validated for TKA) during simulated gait (GT), deep knee bending (DKB), and stair descent (SD). The implant–bone interface micromotion and the ideal area for bone ingrowth for each model were predicted and compared with the original configuration.

2 Methods

2.1 Computational Modeling. A novel fixed-bearing cementless UKA prototype (a medial UKA component) was used in this study. The cementless concept is a modification of the cemented SIGMA HP Partial Knee (DePuy Synthes, Warsaw, IN). The implant–bone contact surface includes a three-dimensional-printed titanium porous coating. The femoral component has a twin-peg design, and the tibial baseplate uses a straight keel and a single peg for enhancing fixation (Fig. 1(*a*)).

Three deformable knee models (all Caucasian females; age: 62.3±11.4 yr; height: 158.2±1.3 cm; and weight: 66.0±22.7 kg) were developed in ABAQUS/STANDARD (SIMULIA, Providence, RI) to conduct this study. The tibia models were prevalidated and adopted from our previously published work [25]. The descriptions of the experimental–computational validation work are briefly summarized here. Three cadaveric specimens were implanted with cementless TKA implants and tested under GT, DKB, and SD loads using the 6DoF AMTI VIVO^{TM} knee simulator (AMTI, Watertown, MA). Relative displacement between marker couples (placed at the anterior aspects of the tray and bone) and tibial bone surface displacements were recorded with a digital image correlation system. Corresponding subject-specific finite element models were reconstructed from the experiments and used to predict the marker relative displacements and tibial surface displacements. Elastic moduli of the bone elements were calculated based on Hounsfield units from the CT scans (with bone mineral density phantoms). Experimental measurements were used to validate model estimations. The average root-mean-square differences and correlations between measured marker relative displacements and predictions were 13.1 μm and 0.86, respectively. Root-mean-square differences and correlations between measured tibial bone surface displacements and predictions were 78.9 μm and 0.84. The corresponding femur models were developed from CT scans and assigned the same material properties as those used for the tibia.

The UKA prostheses were virtually implanted into the three knee models (all best-fitting a size-2 design) in HYPERMESH (Altair Engineering, Inc., Troy, MI), using the virtual tool provided by the manufacturer for landmark identifications and bone resections (tray: perpendicular to sagittal plan, 4 mm depth from dwell point, and patient posterior slope; femoral: perpendicular to sagittal plan, parallel to full extension transverse plan, and matching patient condylar curve) (Fig. 1(*b*)). The UKA components, femur, and tibial bones were meshed with first-order tetrahedral elements. Femoral and tibial cartilages in the lateral compartment were reconstructed from the bony surfaces and were meshed with hexahedral elements using a semi-automated morphing technique [28]. The cartilage was assumed to have a uniform thickness, with equal thickness for both tibial and femoral cartilage, filling the gap between the bones in the full extension scans. All components were deformable and were modeled as linearly elastic with different material properties, except cartilage, which was assigned incompressible hyperelastic material properties using the first-order Ogden strain energy potential model [29] (Table 1). For each bone element, the density was determined from Hounsfield units (calibrated with a phantom), and the corresponding elasticity was calculated using an established relationship [30]. The mesh sizes and the number of materials to characterize bone properties were identified from convergence studies in our previous work [25] and were also adopted here (Table 1). The interactions between the bone and cementless implant surfaces were assumed to be line-to-line (no interference fit) and modeled with a 1.0 friction coefficient based on test data from the manufacturer. The contact at the metal–poly (femoral–insert and insert–tray) interfaces was modeled with friction coefficients of 0.04 [31]. The cruciate ligaments and the other knee soft tissues were not directly represented as the model was kinematically controlled in the degrees-of-freedom (DoF) constrained by soft tissue. It should be noted that the porous coating was not modeled separately, as the coating thickness was not specified for this design at this stage. The cementless contact was simulated using realistic, tested friction coefficients, though the material properties of the porous coating were not applied. However, a complementary test was conducted and demonstrated less than a 5% difference in micromotion, with slightly higher micromotion observed when the porous coating was modeled and given its material properties.

The design-specific kinematics during GT, DKB, and SD activities were adopted from a published study [32] (size-2 data provided directly by the affiliation of the published study), where knee kinematics during daily activities were tracked from ten patients (without anterior cruciate ligament deficient) implanted with the cemented version of the UKA design, using a mobile single-plane fluoroscope. The transformations between the femoral and tibial components were resolved using a Grood and Suntay kinematic description [33], and only the data from patients with size-2 implants were averaged and used in this study (to keep consistent with the computational specimens). For each activity, the design-specific AP, medial–lateral (ML), internal–external (IE), and flexion–extension (FE) kinematics were applied through the Grood and Suntay system to drive the computational models, which exactly reproduced the femoral–insert relative motion measured in vivo. The corresponding superior–inferior (SI) and varus–valgus (VV) loads were estimated using a previously validated lower limb model [34] and were also applied through the Grood and Suntay system. The lower limb model is a proportional–integral–derivative controlled knee simulator designed to replicate in vivo loading conditions across various activities and boundary conditions. By controlling the primary lower limb muscle groups, the model adapts to changes in component design to consistently reproduce target kinematics.

The applied kinematics and loading boundary conditions were consistent across all three knee models, which are shown in Fig. 2. Patellofemoral forces were not considered in the analysis as the design does not typically involve patellar contact with the femoral components during the simulated activities.

The three original knee models (indicated as *baseline* models subsequently) were then perturbed to investigate the sensitivities of implant–bone interface micromotions to specific UKA factors. For each factor studied, the change of the factor was incorporated into each baseline model, and the newly generated model was retested during GT, DKB, and SD. The parameters of each factor and corresponding model configurations are described below.

2.2 Unicompartmental Knee Arthroplasty-Specific Factors

2.2.1 Implant–Bone Alignment. Tray–bone alignment: For each baseline model, four models were developed by perturbing the initial tray–bone alignment (considering one perturbation at a time) ± 1 mm in the AP and ML translational DoFs (Fig. 3). The AP and ML perturbations were relatively small to prevent excessive implant–bone overhang given the appropriate sizing and fit of the neutral implanted trays.

Table 1 Material properties used in the computational models

Components	Density (g/cm^3)	Elastic moduli (MPa)	Poisson's ratios	Mesh density
Femoral—Titanium	4.50	110,000	0.31	1 mm
Tray—Titanium	4.50	110,000	0.31	1 mm
Insert—Polyethylene	0.94	571.6	0.45	1 mm
Cortical bone	$\geq$1	$\leq$9922.6	0.3	0.75 mm at interface, 1.5 mm on the surface
Trabecular bone	$\leq$1	$\geq$79.6	0.3	0.75 mm at interface, 1.5 mm on the surface
Bone cartilage	1.1	Hyperelastic: First-order Ogden strain energy potential model ($\mu_0 = 0.87$ MPa, $\alpha_1 = 14.84$, and $D_1 = 0.03$) [29]		

Approximately 400 material properties were used for modeling the bones (one material property per 4 mg/cm^3 bone apparent density).

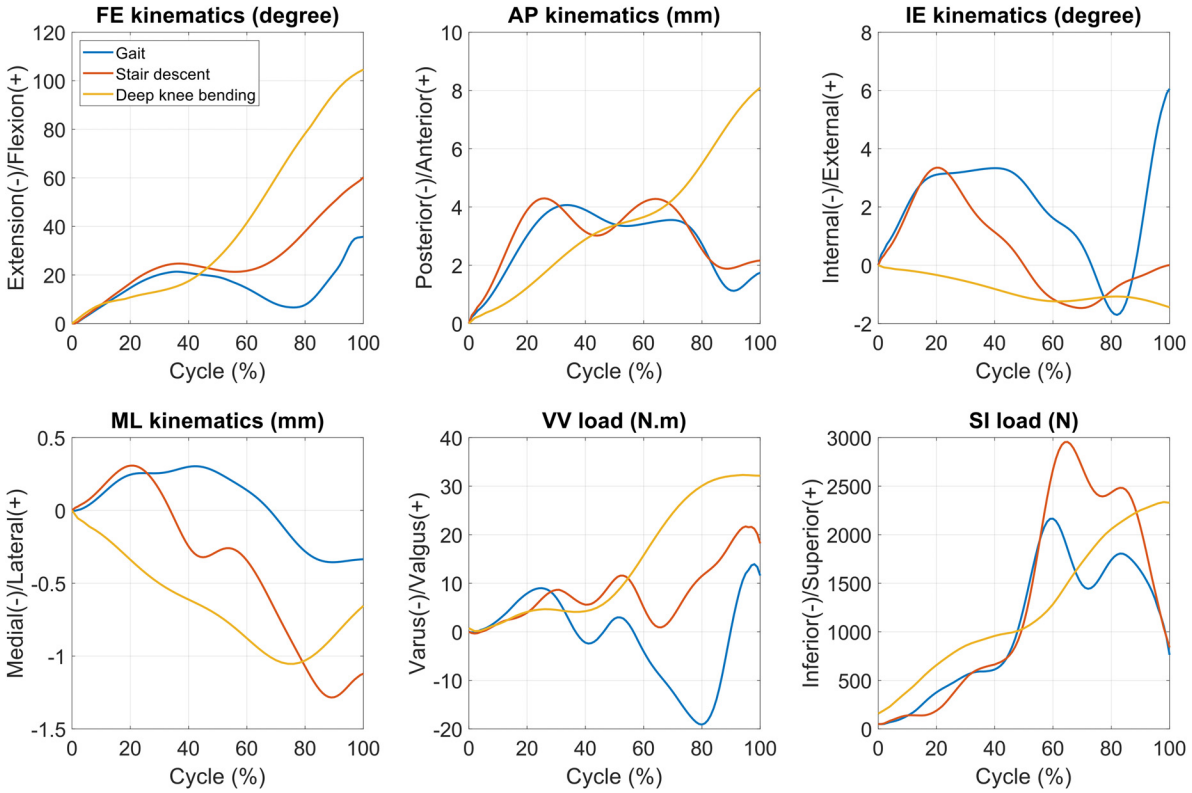

Fig. 2 The tibiofemoral kinematics and loading profiles applied to the Grood and Suntay system of the knee model

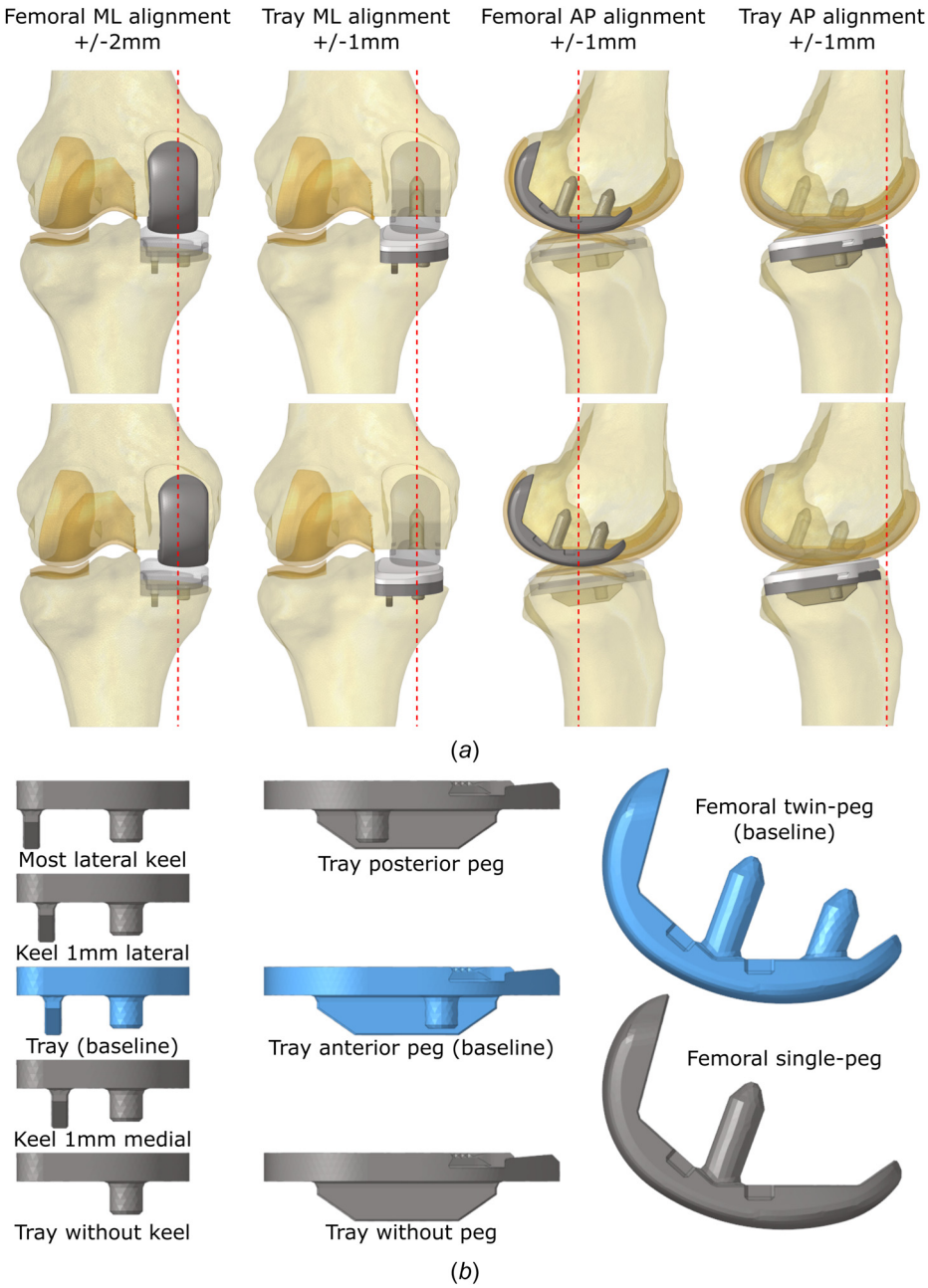

Fig. 3 (*a*) Implant–bone alignment variations (left knee sample) and (*b*) implant design variations

Femoral–bone alignment: For each baseline model, six models were developed by perturbing the initial femoral–bone alignment ±1 mm in the AP and ±1 mm and ±2 mm in the ML translational DoFs (Fig. 3). Larger femoral–bone ML translations could be accommodated without introducing overhang.

It should be noted that our study aimed to explore how deliberate changes in alignment could be optimized to reduce micromotion, rather than evaluating the impact of inherent surgical variability. The perturbation values were chosen to avoid causing excessive overhang.

2.2.2 Bone Material Properties. Up to 53% difference in bone elasticity between samples with the same bone volume fraction has been reported due to the different trabecular architectures [35]. In order to evaluate the potential impact of variation in material properties, the elastic properties of the bone elements were recalculated using both lower- and upper-bound elastic–density relationships reported in the literature [30,36]. For example, bone apparent density ranging from 0.1 to 1.7 g/cm^3 corresponded to elastic moduli of 54 MPa–10 GPa and 372 MPa–17 GPa when using the lower- and upper-bound elastic–density relationships, respectively.

2.2.3 Tibiofemoral Anterior–Posterior Translation. Anterior–posterior translations of the contact point between the femur and tibia had a considerable impact on micromotion in TKA [27]. To study the impact of tibiofemoral AP translations on micromotion in UKA, we scaled the posterior translation of the medial femoral condyle during each activity to increase the peak posterior translation by 0–5 mm (with 1 mm increments) [37].

2.2.4 Implant Design Factors. Cementless implant–bone coefficient of friction: Based on the test data from the manufacturer, the coefficient of friction was defined as 1.0 at the cementless implant–bone interface for the baseline model. To study the impact

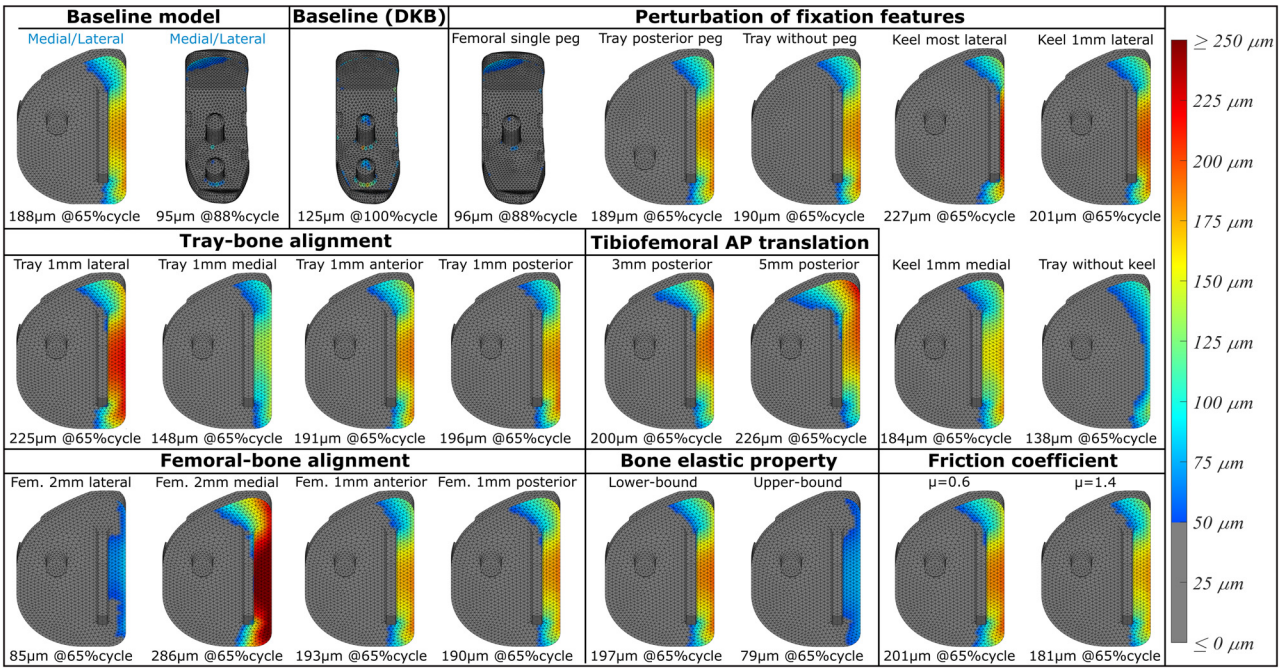

Fig. 4 The full-field interface micromotion contour maps at the frames having peak micromotion magnitudes for the baseline model and the typical perturbation models of each factor (the presented plots were from the second specimen during stair descent activity)

of this factor, the coefficient of friction was perturbed from 0.6 to 1.4 (with 0.2 increments) to cover a wide range of potential variability.

Tray fixation features: To study the impact of the keel, we perturbed the keel position ±1 mm in the ML direction. We also simulated the extreme cases where the keel was placed at the lateral border of the tray and removed completely. To study the impact of the tray peg, tray models were created by removing the peg and flipping the peg in the AP direction (10.4 mm more posterior) (Fig. 3).

Femoral component fixation features: A previous study reported no difference in cemented micromotion between single-peg and twin-peg designs [23]. In this study, we also removed the anterior peg of the femoral component to study the impact on cementless micromotion (Fig. 3).

Overall, a total of 87 models (three baseline models and 84 perturbation models) were created and 261 simulations (87 models tested under three loading conditions) were conducted to complete this study.

2.3 Data Analysis. Implant–bone interface micromotion was defined as the change in the distance (incorporating both normal and shear components) between the nodes on the implant porous surface and the nearest nodes on the bone implantation surface. For each model, the micromotion at the femoral–bone and tray–bone interface was predicted throughout the entire activity cycle. The full-field micromotion across the cementless contact surface was calculated, and the contour maps for the frame having the peak micromotion were presented.

Since a design with larger peak micromotion could have a greater extent of osseointegration [27,38], we also investigated the porous surface area favorable for bone ingrowth (micromotion less than 50 μm, indicated as SA $<$ 50 μm) [39] as another indicator of the fixation strength. The impact of each factor on the micromotion was determined by comparing the maximum interface micromotion over the cycle and the optimal ingrowth area (SA $<$ 50 μm) to the baseline models. The changes in contact surface area due to alignment perturbations were not considered for comparison purposes. In the worst-case scenario, the overhang areas in the models are 2.2% for the tibial tray and 0.8% for the femoral components, which are considered negligible and not expected to impact the results.

3 Results

For visualization of the resulting micromotion, the full-field interface micromotion contour maps for each factor are presented for one of the three specimens during SD activity (SD activity consistently had the highest micromotions comparing with the GT and DKB) (Fig. 4). The contour maps for the other two specimens are provided in the Supplemental Materials on the ASME Digital Collection (Figs. S1 and S2), as the effect of each studied factor on micromotion remained consistent across specimens, with variations only in the micromotion magnitudes. The patterns of the micromotion were similar during DKB and GT activities but of lower in magnitude. The femoral–bone micromotion contour maps are only shown for select factors since the magnitude and distribution of the femoral–bone micromotion were consistent across model configurations.

Overall, the peak *tray*–bone micromotion (187±46 μm, occurring during SD) was consistently higher than the *femoral*–bone micromotion (134±8 μm, occurring during DKB). For the tray–bone interface, the peak micromotion was consistently found along the lateral edge of the tray for all activities. The minimum percentage of the porous surface area ideal for bone ingrowth ranged from 74.1% (SD activity) to 86.6% (DKB activity). Specifically, the tray–bone micromotion along the lateral edge was predominantly shear in the ML direction, while liftoff micromotion occurred at the anterolateral aspect, with its magnitude influenced by the femoral–insert AP contact location. The ratio of shear to liftoff micromotion was approximately 4:1. For the femoral–bone interface, peak micromotion occurred at the posteromedial edge of the femoral components during GT and SD activities (Fig. 4). Although the DKB activity generated higher femoral–bone interface micromotion than the other two activities, the micromotions mainly occurred on the pegs (Fig. 4—baseline DKB). The percentage of the femoral porous area favorable for bone ingrowth was greater than 95% throughout the DKB activity, which was similar to GT and SD activities (93–100%), and much higher than the tray–bone interface. Specifically, the femoral–bone micromotion at the posteromedial

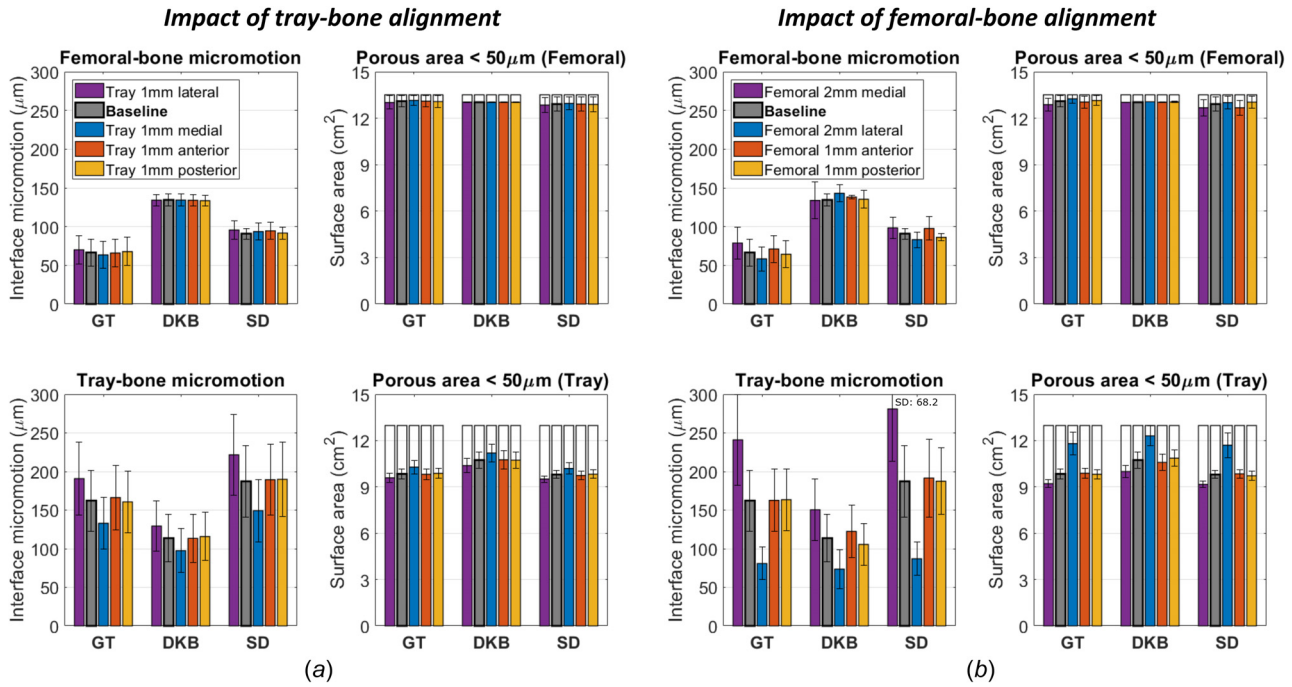

Fig. 5 Impact of tray–bone (*a*) and femoral–bone alignment (*b*) on the interface micromotions and porous coating area ideal for bone ingrowth (mean±SD). The empty bars in each right plot represent the total porous coating area of the corresponding model.

edge was shear micromotion, while micromotion at the pegs was along the SI direction. The impacts of each factor on the interface micromotion and contact area ideal for bone ingrowth are listed below.

3.1 Implant–Bone Alignment. *Tray–bone alignment*: Perturbations of the tray alignment in the lateral direction resulted in an average 19.3% increase in peak tray–bone interface micromotions, occurring during SD, and a corresponding 3.5% reduction in SA $< 50\ \mu$m per 1.0 mm of translation. Micromotion changes caused by alignment perturbations along the AP direction were negligible (1.3% and 0.4% in tray–bone micromotions and SA $< 50\ \mu$m, respectively) (Fig. 5(*a*)). Implanting the tray medially always resulted in lower tray–bone interface micromotions and higher SA $< 50\ \mu$m for all specimens. Perturbation of tray–bone alignments had no impact on the femoral–bone interface micromotion within the bounds of the perturbation studied (Fig. 5(*a*)).

Femoral–bone alignment: Perturbations of the femoral component alignment in the medial direction resulted in a 26.3% increase in peak tray–bone interface micromotions and corresponding 5.5% reduction in the SA $< 50\ \mu$m per 1.0 mm of translation. The average change caused by perturbations along the AP direction was negligible (1.2% and 0.6% in tray–bone micromotions and SA $< 50\ \mu$m, respectively) (Fig. 5(*b*)). Implanting the femoral component laterally always resulted in lower tray–bone interface micromotions and higher SA $< 50\ \mu$m for all specimens. Perturbation of femoral–bone alignment had a much smaller impact on the peak femoral–bone interface micromotion (3.6% due to ML perturbation per 1 mm of translation; 1.7% for AP perturbation) (Fig. 5(*b*)).

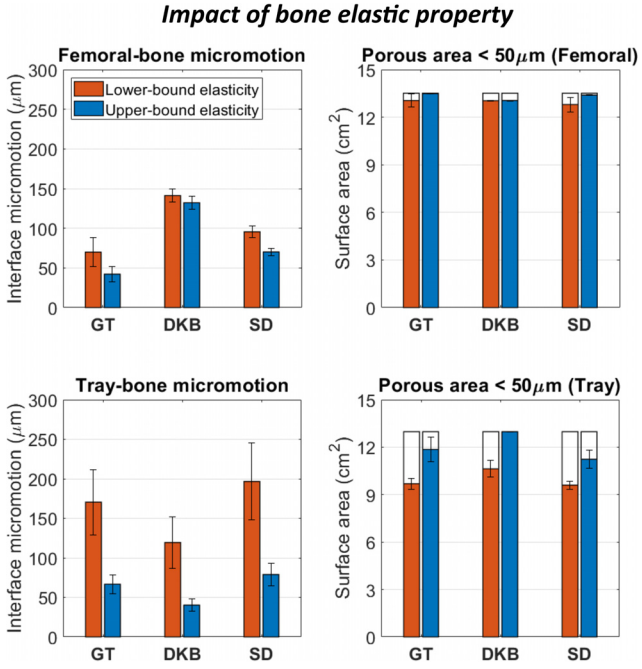

Fig. 6 Impact of bone material properties on the interface micromotions and porous coating area ideal for bone ingrowth (mean±SD)

3.2 Bone Material Properties. The differences in the peak tray–bone interface micromotion and corresponding SA $< 50\ \mu$m between models using upper- and lower-bound elastic material properties were on average 59.8% and 17.0%, respectively. The differences in the peak femoral–bone interface micromotion (6.4%) and the minimum SA $< 50\ \mu$m (0.1%) were much smaller (Fig. 6).

3.3 Tibiofemoral Anterior–Posterior Translation. The peak tray–bone interface micromotion gradually increased with the posterior translation of the femoral condyle, showing an average increase of 35.8% for a 5 mm posterior translation. The corresponding SA $< 50\ \mu$m decreased by an average of 5.7%. The differences in the peak femoral–bone interface micromotion (3.7%) and the minimum SA $< 50\ \mu$m (0.1%) were negligible (Fig. 7(*a*)).

3.4 Implant Design Factors. *Cementless implant–bone coefficient of friction*: The peak tray–bone micromotions reduced by an average of 10.4% when increasing the coefficient of friction from

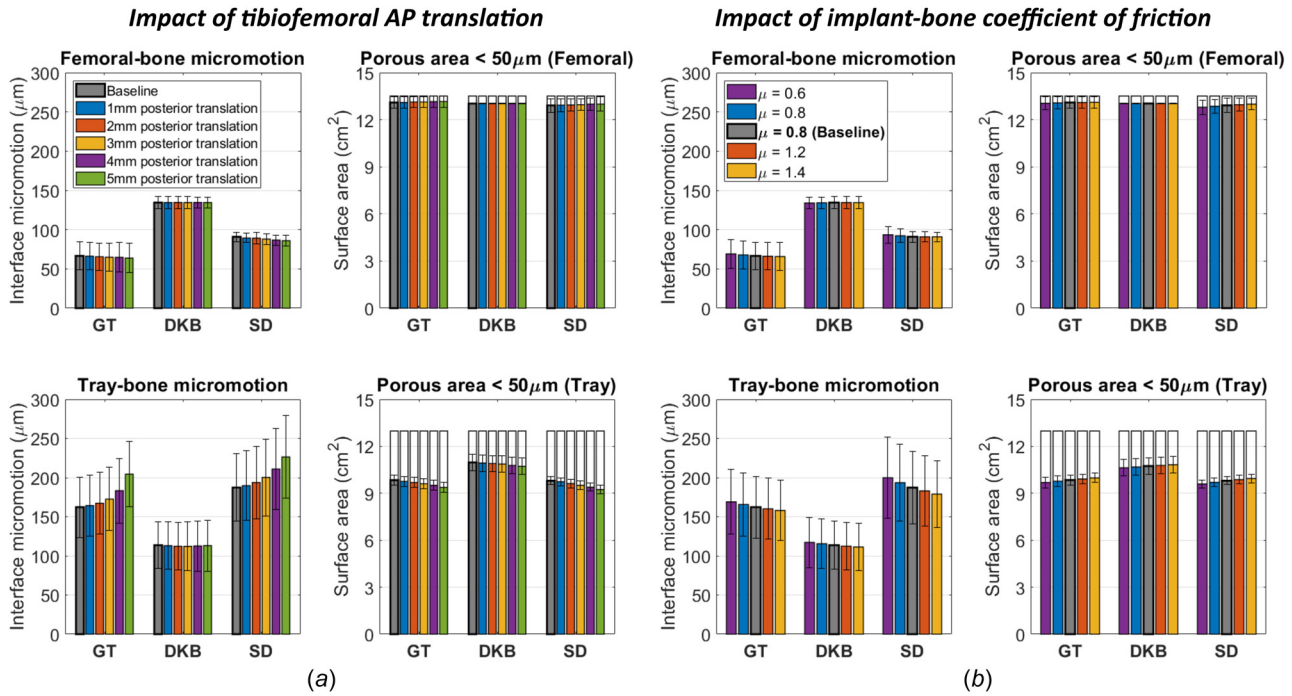

Fig. 7 Impact of tibiofemoral AP translation (*a*) and implant–bone coefficient of friction (*b*) on the interface micromotions and porous coating area ideal for bone ingrowth (mean±SD)

0.6 to 1.4, and the corresponding SA < 50 μm increased by an average of 3.6%. Perturbation of the contact coefficient of friction has a negligible effect on the femoral–bone interface micromotion (Fig. 7(*b*)).

Tray fixation features: The peak tray–bone interface micromotion decreased slightly when moving the keel medially, at an average rate of 4.90% per 1 mm of medial translation. However, the corresponding SA < 50 μm decreased simultaneously at an average rate of 2.7% per 1 mm of medial translation (Fig. 8(*a*)). The minimum peak tray–bone micromotion (143±39 μm) was achieved when the keel was removed, which was on average 35.9% smaller than the model with the most lateral keel. However, the corresponding SA < 50 μm of the model without the keel was significantly smaller (18.4%) than the model with the most lateral keel. The impact of the peg position on the peak tray–bone interface micromotion was negligible (Fig. 8(*b*)). However, the tray SA < 50 μm was reduced by 6.7% due to the removal of the tray peg. The tray fixation features had no impact on the femoral–bone micromotion.

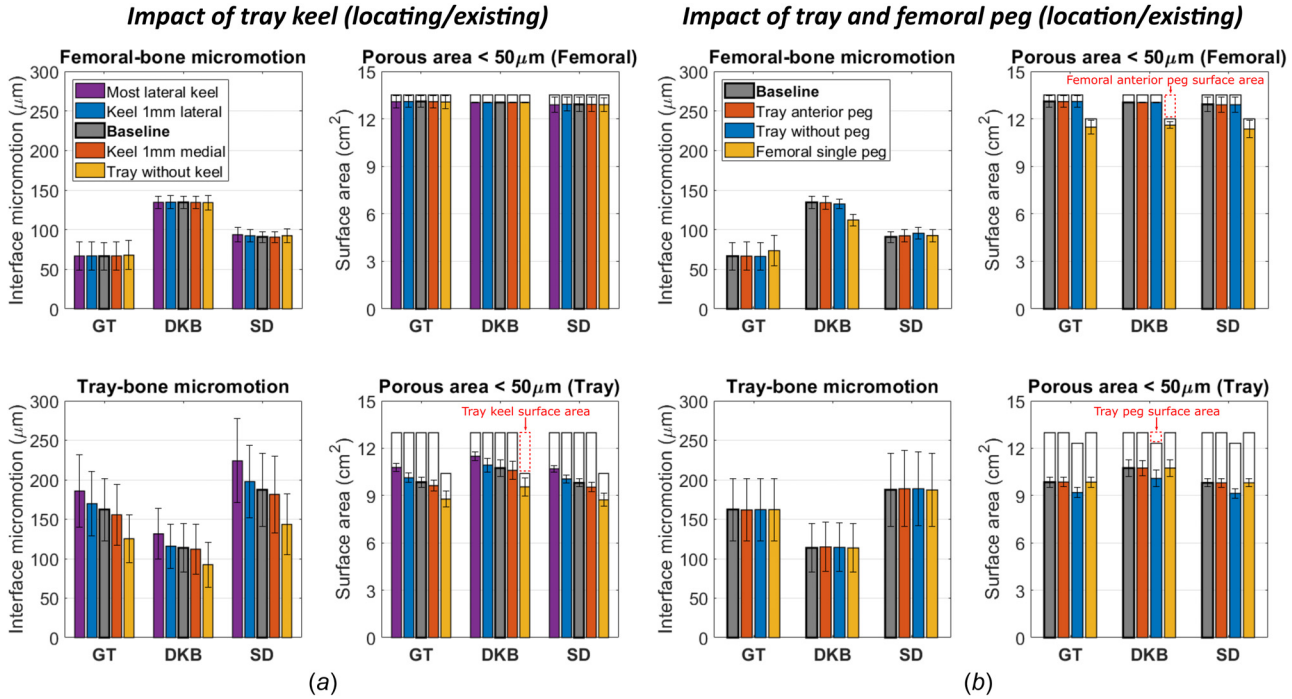

Fig. 8 Impact of tray keel (*a*) and tray and femoral peg (*b*) on the interface micromotions and porous coating area ideal for bone ingrowth (mean±SD)

Femoral component fixation features: Higher micromotion occurred on the anterior peg of the femoral component compared to the middle peg (Fig. 4—baseline DKB). Removal of the femoral anterior peg reduced the femoral–bone micromotion by an average of 16.5% compared with the twin-peg design. However, the minimum SA $< 50\,\mu$m of the femoral component reduced by 12.0% due to the removal of the peg. The femoral anterior peg had no impact on the tray–bone micromotion (Fig. 8(*b*)).

The impact of each factor on the implant–bone micromotion and the corresponding SA $< 50\,\mu$m is listed in Table 2.

4 Discussion

The primary fixation of cementless knee replacement relies on bone ingrowth into the porous surface of the implants. In this study, we investigated the implant–bone interface micromotion and the surface area favorable for bone ingrowth for a novel cementless UKA design during three activities of daily living. Specifically, we assessed the impact of implant–bone alignment, bone material properties, tibiofemoral AP translation, and implant design factors on micromotion. Three cadaveric knee models (tibia models were previously validated for predicting cementless TKA micromotion) were utilized to conduct this study, and design-specific kinematics were applied to actuate the models.

A previous study that experimentally measured tray–bone surface displacements for a similar UKA design (Oxford cementless, Zimmer Biomet, Warsaw, IN) [24] reported maximum micromotion at the anterolateral edge of the tray, with a decrease toward the medial side. Although that study focused on a mobile bearing design, the observed trend remains applicable to the fixed bearing design used in our study, owing to its flat articular surface and unrestricted range of motion. In our study, the predicted tray–bone micromotion distribution follows the same trend at those specific locations (Fig. 4). However, the peak tray–bone interface micromotion (during SD activity) consistently occurred at the lateral edge of the tray. It is important to note that the potential location of maximum micromotion (along the lateral edge) could not be experimentally measured, leaving it unverified by existing experimental data. This limitation underscores the importance of computational simulations in complementing experimental methods. Our predicted femoral–bone micromotion distribution pattern (Fig. 4) was also in agreement with an experimental study [23] which reported consistently less than 30 μm micromotion along the medial edge of the femoral component. However, those experimental measurements were limited to a few isolated points, and the locations theoretically having the peak micromotions (tibial tray lateral edge and femoral pegs) cannot be measured experimentally since they were either occluded by bony tissues or inside the bone. This highlights the necessity of using computational models to assess cementless fixation in UKA.

In this study, the peak tray–bone interface micromotions ($187 \pm 46\,\mu$m) were consistently higher than the femoral–bone micromotions ($134 \pm 8\,\mu$m). The minimum percentage of the porous area ideal for bone ingrowth was $95.6 \pm 3.6\%$ for the femoral component, which was much larger than that for the tibial tray ($75.7 \pm 2.0\%$). Also, we found that the femoral–bone micromotion was insensitive to almost all the factors studied. Even in the case of large differences in bone elastic properties, the peak femoral–bone interface micromotion only changed by 6.4%, whereas the tray–bone micromotion changed by 59.8% under the same condition. These findings could explain why loosening is more commonly reported for the tibia in UKA [40,41]. The difference in micromotion and sensitivity between the tray–bone interface and femoral–bone interface was due to the different contact conditions. For the tibial components, the femoral–insert contact point varies on the insert surface during activities. The tibial components experience eccentric loading by the femoral component when the contact location is close to the insert edge, which creates a significant moment on the bone interface. While for the femoral component, the contact point is generally on the J-curve (close to the middle in the ML direction), and thus the component does not typically see eccentric loading during activities. Moreover, the angular cementless surfaces of the femoral component provide additional resistance to micromotion. In summary, the source of the tray–bone micromotion was mainly tray rotation under eccentric loading, while the source of the femoral–bone micromotion was primarily bone deformation at the complex contact regions. Therefore, although the peak femoral–bone interface micromotion ($135 \pm 8\,\mu$m) was higher than the tray–bone micromotion ($114 \pm 31\,\mu$m) during DKB activity, the high femoral–bone micromotion was isolated to a small area on the pegs, and the corresponding SA $< 50\,\mu$m for the femoral component ($96.5 \pm 0.1\%$) was still much larger than that for the tibial tray ($82.7 \pm 4.2\%$). This implies that the micromotion caused by eccentric loading is likely more harmful to cementless fixation, and more efforts should be focused on minimizing tray–bone micromotion.

The implant–bone ML alignment had a significant impact on the tray–bone interface micromotions in UKA. Specifically, we found that implanting the tibial baseplate medially and implanting the femoral component laterally reduced the tray–bone micromotion for all specimens tested. This was because these alignments centralized the load transferred to the tibial baseplate by the femoral component, thereby reducing lifting of the tray along the lateral edge. We also found that the impact of femoral–bone ML alignment on the micromotion (26.3% per 1 mm variation) was greater than that of tray–bone ML alignment (19.3%) with the same perturbation magnitude. The difference was thought to be because perturbation of the femoral–bone alignment also altered the load transfer with respect to the tibial shaft. Implanting the femoral component

Table 2 The sensitivity of implant–bone micromotions and corresponding SA < 50 μm to each of the factors studied; the values larger than 5% were highlighted

Factor	Peak tray–bone micromotion (%)	Minimum tray SA < 50 (%)	Peak femoral–bone micromotion (%)	Minimum femoral SA < 50 (%)
Tray ML alignment (per 1 mm)	**19.29**	3.48	0.23	0.42
Tray AP alignment (per 1 mm)	1.26	0.42	0.56	0.09
Femoral ML alignment (per 1 mm)	**26.28**	**5.54**	3.64	0.64
Femoral AP alignment (per 1 mm)	1.16	0.64	1.65	1.40
Bone elastic properties	**59.84**	**17.02**	**6.40**	0.11
Tibiofemoral AP translation (5 mm)	**35.81**	**5.69**	3.66	0.07
Coefficient of friction (per 0.1)	1.74	0.60	0.06	0.26
Tray keel ML positioning (per 1 mm)	4.89	2.68	No impact	No impact
Tray keel (presence)	**35.94**	**18.39**	No impact	No impact
Tray peg (presence)	0.72	**6.74**	No impact	No impact
Femoral anterior peg (presence)	No impact	No impact	16.54[a]	**12.04**

[a]The impact of the femoral anterior peg on the micromotion was considered negligible because the peak micromotion occurred at the anterior peg, and the micromotion elsewhere on the femoral component was unchanged after the removal of the anterior peg.

centrally would also centralize the load transferred on the tibia, which reduced the tibial bending moment and thereby contributed to minimizing the tray rotation. However, implanting the tibial tray centrally does not change the bending moment on the tibia, which resulted in a relatively smaller impact on the micromotion. Our finding indicated that the cementless fixation in UKA can be improved by optimizing the implant–bone ML alignment. Since the tray–bone alignment is likely small in the ML direction given a properly sized and implanted tray, perturbation in tray–bone ML alignment could cause a undesired under/overhang. Therefore, optimizing the femoral–bone ML alignment should be preferred to minimize tray–bone micromotion as the positioning of the femoral component is more variable. However, it should be noted that the excessive centralization of the femoral component might cause excessive forces lateral to the keel and result in the tibial baseplate subsiding into a valgus position [42].

Our previous study in TKA found that a more posterior femoral–insert contact causes greater tray tilt, leading to a significant increase in micromotion at the anterior aspect of the tray [26,27]. This finding held true in UKA as well (Fig. 4—tibiofemoral AP translation). However, the effectiveness of attempting to reduce micromotion by controlling the tibiofemoral AP translation was limited (Fig. 7(*a*)), This limitation arises because moving the contact anteriorly only eliminates the anterior lifting, while the micromotion caused by moments impacting medial and lateral edges persist. In contrast, the tray–bone micromotion can be effectively reduced by centralizing the AP contact locations in TKA.

Implant design factors affected the cementless UKA fixation in different ways. The coefficient of friction had a small impact on the tray–bone micromotion over the wide range studied. But clearly, intentionally increasing friction will aid in minimizing the tray–bone micromotion. Regarding the fixation features, the tray keel played an important role in tibial fixation, while the tray peg and the femoral anterior peg had no impact on the micromotion of their respective implants. A previous experimental study also reported no difference in the relative micromotion at the femoral–bone interface between the single-peg and twin-peg femoral designs [23]. However, the existence of these fixation features did increase the total porous surface area ideal for bone ingrowth, which in turn strengthened the overall fixation stability. Also, a second femoral peg could provide additional fixation unrelated to micromotion (such as resistant to spin), which was not discussed here. For the tray keel, lateralization of the keel location resulted in higher tray–bone interface micromotion (Fig. 8). However, the resulting surface area ideal for bone ingrowth ($SA < 50\ \mu m$) also increased, which indicated stronger fixation stability. On the contrary, adjusting the keel location medially resulted in lower tray–bone micromotion but also decreased the porous area favorable for bone ingrowth (Fig. 8), which indicated weaker fixation stability. This finding was in line with previous studies that reported the design with larger micromotion could have a greater extent of osseointegration [27,38], which implies that solely investigating the peak interface micromotion is not enough to evaluate the implant fixation performance. The presence of the tray keel effectively prevented the spread of micromotion over the keel (Fig. 4) and increased the total porous surface area, even with the increased micromotion lateral to the keel. Hence, we suggest future work investigating porous areas favorable for bone ingrowth as the priority indicator to assess cementless fixation.

Differences in the bone material properties between models had a substantial impact on the tray–bone micromotion but a much smaller impact on the femoral–bone micromotion (Fig. 6). The difference in peak tray–bone interface micromotions were up to 59.8% over the range of bone elasticity evaluated. This may partially explain why tibial loosening is more common in UKA [40,41]. However, these differences in bone quality exist between patients and must be accommodated by the implant. Therefore, minimizing the tray–bone interface micromotion through implant design and surgical technique are critical to prevent implant loosening and improve survivorship in UKA in patients with poor quality bone.

It should be noted that this study focused on UKA. Since the medial condyle typically exhibits less posterior rollback than the lateral condyle, the bending moment around the tibial ML axis was relatively small. Therefore, we did not see as much anterior tray liftoff as in our previous study of TKA tibial trays [25–27]. However, for a lateral UKA, the micromotion distribution and sensitivity could be different due to greater posterior translation of the lateral condyle. A more comprehensive study focused on lateral UKA is thus required in the future.

This study has limitations to note. First, the computational analysis was based on three validated tibia specimens for predicting implant–bone micromotion in TKA. The femur models were developed using the same material properties as the corresponding validated tibia models. Although design-specific kinematics and loadings were applied, direct experimental validation on the micromotion results has not been performed for this UKA study. However, the bones were implanted following the manufacturer's guidelines, which gives us confidence in the accuracy of its alignment. Additionally, our predicted micromotion patterns were comparable with previous experimental studies on similar UKA designs even though the locations potentially exhibiting the peak micromotions were not measured. Future experimental studies are expected to measure the micromotion at the lateral edge of the tray. Second, standardized kinematics and loading profiles were used in this study. Variations in kinematics and loading due to individual anatomy, implant alignment, and soft tissue balance were not considered, which could influence micromotion magnitude and distribution. However, the impacts of the studied factors are expected to remain consistent as the mechanisms are unchanged. Centralizing load transfer, minimizing the bending moment on the tibia, and increasing the overall porous coating area are consistent themes that contribute to improving cementless fixation. Third, the implant alignment perturbations may alter the kinematics and loading conditions, which was not considered in this study. Nevertheless, since the insert used in this study has a relatively flat articulation surface, the variations in boundary conditions resulting from the studied perturbation magnitudes are expected to be minimal. Subsequently, only one implant design was considered. The external boundary conditions and resulting sensitivities may be different for other implant designs. Future work could leverage the current computational framework to study other implant designs. Finally, no interference fit was assumed between the prostheses and the bone, which would likely reduce the predicted levels of micromotion.

This study assessed the impacts of implant alignment, bone material properties, and implant design factors on the implant–bone interface micromotion and the surface area ideal for bone ingrowth in UKA. Less concern should be focused on femoral fixation since the femoral–bone micromotion was much smaller than the tray–bone micromotion and was insensitive to almost all the factors studied. The impact of bone properties between individuals on tray–bone micromotion was significant and must be accommodated through robust tray design and appropriate patient selection. The implant–bone alignment in the medial–lateral direction had a considerable impact on the tray–bone micromotion. Lateralization of the tray keel resulted in higher micromotion but also increased the surface area favorable for bone ingrowth. There are clear recommendations for minimizing the tray–bone micromotion from this assessment, including centralizing the load transfer where possible with femoral–insert positioning and optimizing the fixation features. Solely investigating the peak interface micromotion was insufficient to evaluate the fixation stability, as designs with larger peak micromotions could also have a greater surface area with area ideal for osseointegration. The workflow presented in this study could be used as a benchmark for investigating other factors and assessing future UKA designs.

Funding Data

- DePuy Synthes Products, LLC (Funder ID: 10.13039/100008426).

Conflict of Interest

Authors (Paul J. Rullkoetter and Chadd W. Clary) received research or institutional support as a principal investigator from DePuy Synthes Products, LLC.

Data Availability Statement

The authors attest that all data for this study are included in the paper.

References

[1] Insall, J., and Walker, P., 1976, "Unicondylar Knee Replacement," Clin. Orthop. Relat. Res., **120**, pp. 83–85.

[2] Patil, S., Colwell, C. W., Jr., Ezzet, K. A., and D'Lima, D. D., 2005, "Can Normal Knee Kinematics Be Restored With Unicompartmental Knee Replacement?," J. Bone Jt. Surg. Am., **87**(2), pp. 332–338.

[3] Laurencin, C. T., Zelicof, S. B., Scott, R. D., and Ewald, F. C., 1991, "Unicompartmental Versus Total Knee Arthroplasty in the Same Patient," Clin. Orthop. Relat. Res., **273**, pp. 151–156.

[4] Wiik, A. V., Manning, V., Strachan, R. K., Amis, A. A., and Cobb, J. P., 2013, "Unicompartmental Knee Arthroplasty Enables Near Normal Gait at Higher Speeds, Unlike Total Knee Arthroplasty," J. Arthroplasty, **28**(9), pp. 176–178.

[5] Hopper, G. P., and Leach, W. J., 2008, "Participation in Sporting Activities Following Knee Replacement: Total Versus Unicompartmental," Knee Surg. Sports Traumatol. Arthrosc., **16**(10), pp. 973–979.

[6] National Joint Registry, 2021, "National Joint Registry for England and Wales. 9th Annual Report," National Joint Registry, London, accessed Nov. 12, 2024, www.hqip.org.uk/wp-content/uploads/2018/02/national-joint-registry-9th-annual-report-2012.pdf

[7] Koskinen, E., Eskelinen, A., Paavolainen, P., Pulkkinen, P., and Remes, V., 2008, "Comparison of Survival and Cost-Effectiveness Between Unicondylar Arthroplasty and Total Knee Arthroplasty in Patients With Primary Osteoarthritis: A Follow-Up Study of 50,493 Knee Replacements From the Finnish Arthroplasty Register," Acta Orthop., **79**(4), pp. 499–507.

[8] Mittal, A., Meshram, P., Kim, W. H., and Kim, T. K., 2020, "Unicompartmental Knee Arthroplasty, an Enigma, and the Ten Enigmas of Medial UKA," J. Orthop. Traumatol., **21**(1), p. 15.

[9] Pandit, H., Liddle, A. D., Kendrick, B. J. L., Jenkins, C., Price, A. J., Gill, H. S., Dodd, C. A. F., and Murray, D. W., 2013, "Improved Fixation in Cementless Unicompartmental Knee Replacement: Five-Year Results of a Randomized Controlled Trial," J. Bone Jt. Surg. Am., **95**(15), pp. 1365–1372.

[10] Kendrick, B. J. L., Kaptein, B. L., Valstar, E. R., Gill, H. S., Jackson, W. F. M., Dodd, C. A. F., Price, A. J., and Murray, D. W., 2015, "Cemented Versus Cementless Oxford Unicompartmental Knee Arthroplasty Using Radiostereometric Analysis: A Randomized Controlled Trial," Bone Jt. J., **97-B**(2), pp. 185–191.

[11] Australian Orthopaedic Association National Joint Replacement Registry, 2013, "Annual Report," AOA, Adelaide, South Africa, accessed Nov. 12, 2024, aoanjrr.sahmri.com/annual-reports-2013

[12] Hamilton, W. G., Collier, M. B., Tarabee, E., McAuley, J. P., Engh, C. A., and Engh, G. A., 2006, "Incidence and Reasons for Reoperation After Minimally Invasive Unicompartmental Knee Arthroplasty," J. Arthroplasty, **21**(2), p. 305.

[13] Pandit, H., Jenkins, C., Beard, D. J., Gallagher, J., Price, A. J., Dodd, C. A. F., Goodfellow, J. W., and Murray, D. W., 2009, "Cementless Oxford Unicompartmental Knee Replacement Shows Reduced Radiolucency at One Year," J. Bone Jt. Surg. Br., **91-B**(2), pp. 185–189.

[14] Horsager, K., Kaptein, B. L., Rømer, L., Jørgensen, P. B., and Stilling, M., 2017, "Dynamic RSA for the Evaluation of Inducible Micromotion of Oxford UKA During Step-Up and Step-Down Motion," Acta Orthop., **88**(3), pp. 275–281.

[15] Dalury, D. F., 2016, "Cementless Total Knee Arthroplasty: Current Concepts Review," Bone Jt. J., **98-B**(7), pp. 867–873.

[16] Nakama, G. Y., Peccin, M. S., Almeida, G. J., de Lira Neto, O., Queiroz, A. A., and Navarro, R. D., 2012, "Cemented, Cementless or Hybrid Fixation Options in Total Knee Arthroplasty for Osteoarthritis and Other Non-Traumatic Diseases," Cochrane Database Syst. Rev., **10**(10), p. CD006193.

[17] Bragdon, C. R., Burke, D., Lowenstein, J. D., O'Connor, D. O., Ramamurti, B., Jasty, M., and Harris, W. H., 1996, "Differences in Stiffness of the Interface Between a Cementless Porous Implant and Cancellous Bone In Vivo in Dogs Due to Varying Amounts of Implant Motion," J. Arthroplasty, **11**(8), pp. 945–951.

[18] Pilliar, R. M., Lee, J. M., and Maniatopoulos, C., 1986, "Observations on the Effect of Movement on Bone Ingrowth Into Porous-Surfaced Implants," Clin. Orthop. Relat. Res., **11**, p. 11.

[19] Engh, C. A., O'Connor, D., Jasty, M., McGovern, T. F., Bobyn, J. D., and Harris, W. H., 1992, "Quantification of Implant Micromotion, Strain Shielding, and Bone Resorption With Porous-Coated Anatomic Medullary Locking Femoral Prostheses," Clin. Orthop. Relat. Res., **285**, pp. 13–29.

[20] Barker, D. S., Tanner, K. E., and Ryd, L., 2005, "A Circumferentially Flanged Tibial Tray Minimizes Bone-Tray Shear Micromotion," Proc. Inst. Mech. Eng., **219**, pp. 449–456.

[21] Hashemi, A., and Shirazi-Adl, A., 2000, "Finite Element Analysis of Tibial Implants—Effect of Fixation Design and Friction Model, Computer Methods in Biomechanics and Biomedical Engineering," Comput. Methods Biomech. Biomed. Eng., **3**(3), pp. 183–201.

[22] Glenday, J. D., Wright, T. M., Lipman, J. D., Sculco, P. K., Mayman, D. J., Vigdorchik, J. M., and Quevedo-Gonzalez, F. J., 2022, "Effect of Varus Alignment on the Bone-Implant Interaction of a Cementless Tibial Baseplate During Gait," J. Orthop. Res., **40**(4), pp. 816–825.

[23] Reiner, T., Jaeger, S., Schwarze, M., Klotz, M. C., Beckmann, N. A., and Bitsch, R. G., 2014, "The Stability of the Femoral Component in the Oxford Unicompartmental Knee Replacement: A Comparison of Single and Twin Peg Designs," Bone Jt. J., **96-B**(7), pp. 896–901.

[24] Yildirim, G., Gopalakrishnan, A., Davignon, R. A., Parker, J. W., Chawla, H., and Pearle, A. D., 2016, "Comparative Fixation and Subsidence Profiles of Cementless Unicompartmental Knee Arthroplasty Implants," J. Arthroplasty, **31**(9), pp. 2019–2024.

[25] Yang, H., Bayoglu, R., Renani, M. S., Behnam, Y., Navacchia, A., Clary, C. W., and Rullkoetter, P. J., 2020, "Validation and Sensitivity of Model-Predicted Proximal Tibial Displacement and Tray Micromotion in Cementless Total Knee Arthroplasty Under Physiological Loading Conditions," J. Mech. Behav. Biomed. Mater., **109**, p. 103793.

[26] Yang, H., Bayoglu, R., Clary, C. W., and Rullkoetter, P. J., 2023, "Impact of Patient, Surgical, and Implant Design Factors on Predicted Tray-Bone Interface Micromotions in Cementless Total Knee Arthroplasty," J. Orthop. Res., **41**(1), pp. 115–129.

[27] Yang, H., Behnam, Y., Clary, C. W., and Rullkoetter, P. J., 2022, "Drivers of Initial Stability in Cementless TKA: Isolating Effects of Tibiofemoral Conformity and Fixation Features," J. Mech. Behav. Biomed. Mater., **136**, p. 105507.

[28] Baldwin, M. A., Langenderfer, J. E., Rullkoetter, P. J., and Laz, P. J., 2010, "Development of Subject-Specific and Statistical Shape Models of the Knee Using an Efficient Segmentation and Mesh Morphing Approach," Comput. Methods Programs Biomed., **97**(3), pp. 232–240.

[29] Weizel, A., Distler, T., Detsch, R., Boccaccini, A. R., Bräuer, L., Paulsen, F., Seitz, H., and Budday, S., 2022, "Hyperelastic Parameter Identification of Human Articular Cartilage and Substitute Materials," J. Mech. Behav. Biomed. Mater., **133**, p. 105292.

[30] Anderson, M. J., Keyak, J. H., and Skinner, H. B., 1992, "Compressive Mechanical Properties of Human Cancellous Bone After Gamma Irradiation," J. Bone Jt. Surg., **74**(5), pp. 747–752.

[31] Godest, A. C., Beaugonin, M., Haug, E., Taylor, M., and Gregson, P. J., 2002, "Simulation of a Knee Joint Replacement During a Gait Cycle Using Explicit Finite Element Analysis," J. Biomech., **35**(2), pp. 267–275.

[32] Zumbrunn, T., Schütz, P., von Knoch, F., Preiss, S., List, R., and Ferguson, S. J., 2020, "Medial Unicompartmental Knee Arthroplasty in ACL-Deficient Knees Is a Viable Treatment Option: In Vivo Kinematic Evaluation Using a Moving Fluoroscope," Knee Surg. Sports Traumatol. Arthrosc., **28**(6), pp. 1765–1773.

[33] Grood, E. S., and Suntay, W. J., 1983, "A Joint Coordinate System for the Clinical Description of Three-Dimensional Motions: Application to the Knee," ASME J. Biomech. Eng., **105**(2), pp. 136–144.

[34] Fitzpatrick, C. K., Baldwin, M. A., Clary, C. W., Maletsky, L. P., and Rullkoetter, P. J., 2014, "Evaluating Knee Replacement Mechanics During ADL With PID-Controlled Dynamic Finite Element Analysis," Comput. Methods Biomech. Biomed. Eng., **17**(4), pp. 360–369.

[35] Ulrich, D., Hildebrand, T., Van Rietbergen, B., Müller, R., and Rüegsegger, P., 1997, "The Quality of Trabecular Bone Evaluated With Micro-Computed Tomography, FEA and Mechanical Testing," Stud. Health Technol. Inf., **40**, pp. 97–112.

[36] Rho, J. Y., Hobatho, M. C., and Ashman, R. B., 1995, "Relations of Mechanical Properties to Density and CT Numbers in Human Bone," Med. Eng. Phys., **17**(5), pp. 347–355.

[37] Kiyohara, M., Hamai, S., Gondo, H., Higaki, H., Ikebe, S., Ushio, T., Murakami, K., and Nakashima, Y., 2020, "Tibiofemoral Kinematics in Healthy and Osteoarthritic Knees During Twisting," J. Orthop., **21**, pp. 213–217.

[38] Chong, D. Y. R., Hansen, U. N., and Amis, A. A., 2016, "Cementless Mis Mini-Keel Prosthesis Reduces Interface Micromotion Versus Standard Stemmed Tibial Components," J. Mech. Med. Biol., **16**(05), p. 1650070.

[39] Grewal, R., Rimmer, M., and Freeman, M., 1992, "Early Migration of Prostheses Related to Long-Term Survivorship. Comparison of Tibial Components in Knee Replacement," J. Bone Jt. Surg. Br., **74-B**(2), pp. 239–242.

[40] Vorlat, P., Putzeys, G., Cottenie, D., Van Isacker, T., Pouliart, N., Handelberg, F., Casteleyn, P., Gheysen, F., and Verdonk, R., 2006, "The Oxford Unicompartmental Knee Prosthesis: An Independent 10-Year Survival Analysis," Knee Surg. Sports Traumatol. Arthrosc., **14**(1), pp. 40–45.

[41] Manson, T. T., Kelly, N. H., Lipman, J. D., Wright, T. M., and Westrich, G. H., 2010, "Unicondylar Knee Retrieval Analysis," J. Arthroplasty, **25**(6), pp. 108–111.

[42] Liddle, A. D., Pandit, H. G., Jenkins, C., Lobenhoffer, P., Jackson, W. F. M., Dodd, C. A. F., and Murray, D. W., 2014, "Valgus Subsidence of the Tibial Component in Cementless Oxford Unicompartmental Knee Replacement," Bone Jt. J., **96-B**(3), pp. 345–349.